International Journal of Pharmaceutics 382 (2009) 234–243

Contents lists available at ScienceDirect

International Journal of Pharmaceutics

journal homepage: www.elsevier.com/locate/ijpharm

Pharmaceutical Nanotechnology

Study on the mechanisms of chitosan and its derivatives used as transdermal penetration enhancers

Wen He*, Xianxi Guo, Lihai Xiao, Min Feng

Department of Pharmacy of Renmin Hospital, Wuhan University, Wuhan 430060, People's Republic of China

ARTICLE INFO

Article history:
Received 13 April 2009
Received in revised form 23 July 2009
Accepted 29 July 2009
Available online 15 August 2009

Keywords:
Chitosan
N-trimethyl chitosan
Mono-N-carboxylmethyl chitosan
Transdermal penetration enhancer
Mechanism

ABSTRACT

The efficacy of chitosan (CS) and its derivatives used as transdermal penetration enhancers has been confirmed in our previous research. This study investigated the mechanisms of penetration enhancement by CS and its derivatives, i.e., N-trimethyl chitosan (TMC) with different degree of quaternization (DQ) and mono-N-carboxylmethyl chitosan (MCC). After treatment with CS, TMCs or MCC, the secondary structure changes of keratin in stratum corneum (SC) from mice were examined by an Attenuated Total Reflection-Fourier Transform Infrared (ATR-FTIR) combined with the application of the second-order derivative, deconvolution and curve-fitting. The water content in the SC was also studied by ATR-FTIR. HaCaT cell lines were employed as the cell models in the study. HaCaT cells were first treated with blank D-Hanks solution, CS or its derivatives, and were then fluorescent labeled with $DiBAC_4$ (3). The change of membrane potential was measured by a flow cytometer (FCM). Alternatively, the treated HaCaT cells were labeled with NBD-C_6-HPC and the change of membrane fluidity was examined under a Confocal Laser Scanning Microscope (CLSM). It was found that CS, TMCs and MCC could significantly affect the secondary structure of keratin in SC in different ways. Although the amide II absorption peak of keratin moved to a lower wave number following treatment with CS, TMCs, or MCC, the β-turning structure of keratin was converted to β-sheeting and random coiling after treatment with TMCs and was converted to β-sheeting and α-helix following treatment with MCC and CS. At the same time, CS and its derivatives all could increase the water content of SC, decrease HaCaT cells membrane potentials and enhance HaCaT cells membrane fluidity significantly. The effect of TMCs appeared to be independent of their DQ. The results suggest that the mechanisms of transdermal enhancement of CS, TMCs and MCC are closely related to their effects on the secondary structure of keratin and water content in SC, cell membrane potential and fluidity.

1. Introduction

Chitosan (CS) is the only polycationic polysaccharide in nature which attracts much interest in pharmaceutical applications. Due to its poor solubility at physiological pH (pH above 6.5), several derivatives of CS have been synthesized which are soluble in a wider pH range. Among them, N-trimethyl chitosan (TMC) and mono-N-carboxymethyl chitosan (MCC) are most frequently studied and used because of their well-defined structures, improved solubility and easy preparation.

Many studies have shown that CS, TMC and MCC could significantly enhance drug absorption across mucosa epithelia (Thanou et al., 2001; Hamman et al., 2002; Jonker et al., 2002; Sinswat and Tengamnuay, 2003; Di Colo et al., 2004; Giuseppina et al., 2005) and the mechanisms have also been clearly elucidated (Junginger and Verhoef, 1998; Kotze et al., 1999; Thanou et al., 2000a,b). However, few studies have been done on the transdermal enhancement of CS and its derivatives. Stratum corneum (SC) of skin is the main barrier against drug transdermal penetration. Although the composition of SC is very different from that of epithelial cells, which is composed of dead keratinized cells and fibrosis protein, SC also has fixed negative charges in the tight junction between cells which are similar to those found in epithelial cells (Hamman et al., 2002). It is therefore reasonable to speculate that CS and its derivatives could be potential transdermal penetration enhancers effective in Transdermal Drug Delivery Systems (TDDS). Recently, it was reported that CS appeared to interact with negative charges in the skin to improve drug diffusion to deeper skin layers (Taveira et al., 2009). Our previous study had also shown that TMC could prominently increase the drug transdermal penetration *in vitro* and *in vivo* (Wen et al., 2008). Despite the above studies, the mechanisms of the transdermal enhancement of CS and its derivatives have not been elucidated.

In this study, after treatment with CS, TMCs or MCC, the secondary structure changes of keratin in stratum corneum (SC) from mice were examined by an Attenuated Total Reflection-Fourier

* Corresponding author.
E-mail address: hwzxd@163.com (W. He).

0378-5173/$ – see front matter © 2009 Elsevier B.V. All rights reserved.
doi:10.1016/j.ijpharm.2009.07.038

Transform Infrared (ATR-FTIR) combined with the application of the second-order derivative, deconvolution and curve-fitting. The water content in the SC was also studied by ATR-FTIR. Also, the water content in SC was studied after treatment by CS and its derivatives using ATR-FTIR determination. HaCaT cells were attempted to be employed as a cell model to study the effect of CS and its derivatives on cell membrane potential and fluidity. Through those studies, the mechanisms of CS and its derivatives used as transdermal penetration enhancers were tried to be explained somewhat.

2. Materials and methods

2.1. General chemicals and polymers

CS (Mw 210 kDa, DD > 95%) from a shrimp shell was bought from Haipu Biotechnology Co. Ltd. (Qingdao, China). Fluorescent probes used were $DiBAC_4$ (3) ([bis-(1,3-dibutylbarbituric acid) trimethine oxonol]) and NBD-C6-HPC ([2-6-(7-nitrobenz-2-oxa-1,3-diazol-4-yl) amino hexanoyl-1-hxadecanoyl-sn-glyxero-3-phosphochline]). All probes were purchased from Invitrogen Incorporation (USA), received in solid form and solubilized in absolute ethanol. All the other chemicals were of analytical grade and used without further purification.

2.2. Mice

Healthy male Kunming species mice weighing 20 ± 2 g were supplied by the Experimental Animal Breading Center of Medical College of Wuhan University. All of the procedures for animal experimentation were performed according to approved protocols and in accordance with recommendations of the NIH guideline for the proper use and care of laboratory animals.

2.3. Cell line

HaCaT cell lines were gifted from the Laboratory of Molecular Biology of Dermatology department (Renmin Hospital of Wuhan University, China). The cells were grown in DMEM, supplemented with 10% (v/v) fetal bovine serum (FBS), 100 units/ml penicillin/streptomycin at 37 °C in a 5% CO_2 incubator. Cells were maintained within their exponential growth phase.

2.4. Synthesis and characterization of TMCs

TMCs with degree of quaternization (DQ) of 20% (TMC20), 40%(TMC40), and 60% (TMC60) were synthesized by varying the number of times and durations of reaction steps as reported by Snyman et al. (2001). Briefly, TMCs were synthesized by reductive methylation of CS through a chemical reaction between CS and iodomethane in the presence of sodium hydroxide. The reaction step was repeated several times with the product obtained from each step to increase the DQ of the TMCs.

All TMCs were characterized by ^{1}H NMR. The products were measured in D_2O at 80 °C, using a 600-MHz spectrometer (Varian unity Inova, USA). The DQ of the synthesized TMCs was calculated with the following equation (Hamman and Kotze, 2001): $DQ(\%) = [(\int TM/\int H) \times (1/9)] \times 100$, where $\int TM$ is the integral of the trimethyl amino group (quaternary amino) peak at 3.3 ppm and $\int H$ is the integral of the ^{1}H peaks from 5.0 to 6.0 ppm.

2.5. Synthesis and characterization of MCC

MCC was synthesized as reported by Di Colo et al. (2004). Briefly, CS was dissolved in 0.7% (v/v) acetic acid solution. Following filtration to remove traces of non-dissolved material, glyoxalic acid was added and the mixture was stirred at room temperature for 90 min. The reaction pH was then brought to 4.5 by addition of 1 M NaOH over 30 min, after which stirring was continued for another 90 min to yield a polymer of imine. Subsequently, the imine was reduced by adding dropwise 5% (w/v) aqueous solution of sodium borohydride and leaving the mixture under stirring at room temperature for 1 h. The polymer was then precipitated by an excess of ethanol and collected by filtration under vacuum. After washing with ethanol and air drying, the product was pulverized by a ball-mill, and then subjected to a second carboxymethylation step using the same procedures as described above. The product was converted into its sodium salt and the solution (pH 10.5) was lyophilized.

MCC was characterized by IR spectroscopy and alkalimetry (Riccardo et al., 1982). 0.2 g MCC was dissolved in 60 ml 0.1 M HCl solution followed by adding pure water to 100 ml. 20 ml sample solution was then taken out to adjust pH to 2.0 with 0.1 M HCl solution and titrated with 0.1 M NaOH solution. Thus the titration curve was constructed.

2.6. Preparation of SC

Mice skin was obtained promptly after post-mortem and carefully shaved with a razor after the removal of hair by electric clippers. Epidermis was gently peeled off by trimming off subcutaneous fat and immersing full thickness skin samples in water. SC sheets were obtained by floating freshly prepared epidermis on an aqueous solution of 0.0001% trypsinase and 0.5% sodium bicarbonate for 24 h. Digested material was removed from the underside of the SC with tissue paper and the isolated sheets were rinsed in acetone for 30 s to remove any sebaceous or subcutaneous fat contamination, cryodesiccated and stored over silica gel under vacuum (Daughety and Mrsny, 1999).

2.7. ATR-FTIR investigation of SC samples

6 mm × 6 mm pieces of dry SC were incubated for 24 h in 3 ml of the respective formulation at room temperature, where the formulation was 2.5% TMC60, 2.5% TMC40, 2.5% TMC20, 2.5% MCC, 2.5% CS and the blank solvent (used as control), respectively. The CS, CMCs and MCC were solubilized in solvent of 100 ml 1% (v/v) acetic acid and then adjusted pH to 6.0 with 0.1 M NaOH solution. Thereafter the SC sheets were cleaned carefully with distilled water to remove all the residual solvent on the SC surface. After cryodesiccation, spectral measurements were made with a Nicolet FTIR 5700 Fourier Transform Infrared Spectrometer (Thermo Nicolet, USA) equipped with a ATR attachment under the following conditions: IR reflection crystal of a diamond monocrystal, scanning temperature range of 18–20 °C, scanning times of 64, resolution of 4 cm^{-1}, and scanning range of 800–4000 cm^{-1}. The curves in each group were recorded and analyzed by the second-order derivative, deconvolution and curve-fitting.

2.8. Determination of water content in SC by ATR-FTIR

6 mm × 6 mm pieces of dry SC were incubated at room temperature in 3 ml of the respective formulation same as described above. At predetermined time intervals (0, 2, 4, 6, 8, 12 h), SC samples were taken out and cleaned carefully with distilled water to remove the residual solvent on the surface. After removing the residual water on the surface of SC with filtering paper, the water content in SC was examined by ATR-FTIR under the conditions described above. The ratio of amide I absorption peak and amide II absorption peak was calculated to define the water content in SC.

2.9. Measurements of membrane potential of HaCaT cells

HaCaT cells, digested into monoplast by 0.5% trypsinase/0.02% EDTA (w/v), were collected and aliquoted. Six formulation groups of 1.0% TMC60, 1.0% TMC40, 1.0% TMC20, 1.0% MCC, 1.0%CS and the blank D-Hanks solution were added into the aliquot, respectively. After incubation for 0.5 h at 37 °C in a 5% CO_2 incubator, the polymers and the solvent were removed from the monoplast and the cell density was adjusted to no less than 10^6 ml^{-1} using PBS (NaCl 8.0 g, KCl 0.2 g, $Na_2HPO_4{\cdot}H_2O$ 1.56 g, KH_2PO_4 0.2 g). Stocking solution of fluorescent probes $DiBAC_4$ (3) was added and incubated for another 0.5 h, where the concentration of $DiBAC_4$ (3) was 5 μg ml^{-1}. The fluorescence intensity was then measured by a Beckman Coulter Epics XL Flow Cytometer (Beckman Co., USA). Excitation/emission wavelength was 488/520 nm, and HaCaT cells without fluorescent label were used as zero adjustment.

2.10. Visualizations of membrane fluidity of HaCaT cells

The cells were seeded on glass slides in 24-cell plate at a seeding cell density of 10^4 cells/cm^2. The above six respective formulation group was added and the plate was incubated for 0.5 h at 37 °C in a 5% CO_2 incubator. After removing the polymers and the solvent, 1 ml NBD-C_6-HPC solution (2 μg ml^{-1}) was added for another incubation of 0.5 h, and then the monolayer of HaCaT cells was withdrawn and put on supporting slides. A method of fluorescence recovery after photobleaching (FRAP) was used here. After the definition of line scanning position, length and photobleaching position, the monolayer was visualized by a Confocal Laser Scanning Microscope (Leica TCS, German) under the following conditions: excitation wavelength of 488 nm, emission wavelength of 530 nm, laser power for fluorescence bleaching of 70%, bleaching time of 0.9 s, scanning frequency of 1.65 s and the total scanning time of 100 s. The fluorescence intensity time-variation at the photobleaching position was recorded and image formation was obtained by confocal tomoscanning. The membrane fluidity was represented by fluorescence recovery rate (R) which was calculated with the following equation (Juan et al., 1982): $R = (F_2 - F_0)/(F_1 - F_0) \times 100$, where F_0 is the instant fluorescence value after photobleaching, F_1 is the fluorescence value before photobleaching and F_2 is the fluorescence recovery value after photobleaching. The greater R is, the better membrane fluidity is.

2.11. Statistical analysis

All experiments in the study were repeated three times except for the synthesis of TMCs and MCC. Data was expressed as the mean value ± S.D. Statistical data was analyzed by one-way analysis of variance (ANOVA). A multiple comparison test was used to compare different groups, and a P-value of 0.05 was considered to be significant.

3. Results and discussion

3.1. Characterization of synthesized TMCs

In Fig. 1, typical ^{1}H NMR spectra of TCM20, TMC40 and TMC60 were depicted. The DQ of TMC20, TMC40, and TMC60 was 25%, 38%, and 59%, respectively. A 0.3 ppm migration towards low chemical shift was observed in our detection as compared with those of standard spectra. Therefore, in the equation $\int H$ is the integral of the ^{1}H peaks from 5.0 to 6.0 ppm instead of 4.7 to 5.7 ppm.

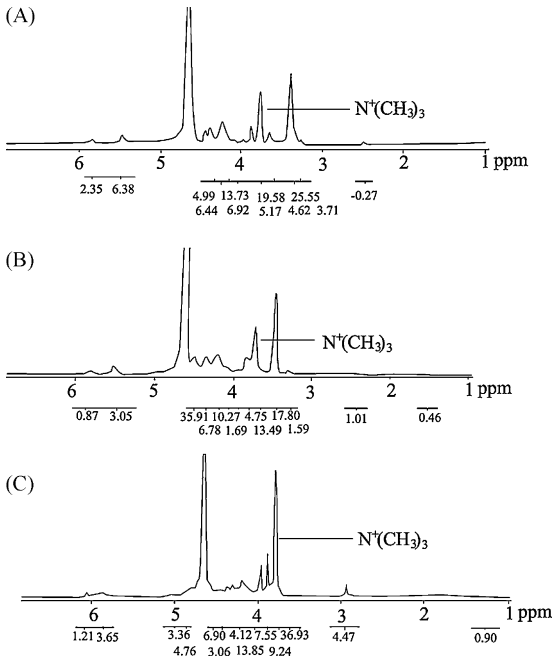

Fig. 1. H NMR spectra of synthesized TMCs (A: TMC20; B: TMC40 and C: TMC60).

3.2. Characterization of synthesized MCC

The IR spectrum of MCC is shown in Fig. 2B. Compared with CS (Fig. 2A), MCC showed the band at 1734 cm^{-1} for υ(C=O) of carboxylic acid, 1635 cm^{-1} and 1375 cm^{-1} for υ(C–N) of tertiary amine. The band around 2900 cm^{-1} was widened also showing the existence of carboxylic acid. Compared with the standard spectrum shown in Fig. 3, the target product was synthesized successfully. The titration curve for MCC is shown in Fig. 4. The second-order derivate was employed to define the consuming volume of NaOH solution at the inflections in the curve and the following equation was used to calculate the substitution degree of MCC: $A = (203.19 \times 7\% + 161.25 \times 93\%) \times N/(M - 80N) \times 93\%$. In the equation, $N = (V_2 - V_1) \times C_{NaOH}$ and M was the molecular quality of MCC (Liu et al., 2004). The curve showed two inflections. The first inflection corresponded to the neutralization of the free acidity of HCl and the attainment of the MCC isoelectric point (pH 2.72), while the second one corresponded to the complete titration of the carboxyl group (pH 5.76). The result showed that MCC with a substitution degree of 57.96% was synthesized.

3.3. Transformation of the secondary structure of keratin in SC under the effect of CS, TMCs and MCC

The main methods for study of the mechanisms of transdermal enhancers are Scanning or Transmission Electron Microscopy (SEM or TEM) (Kuljit and Bhatia, 1999; De Graaff et al., 2003), Attenuated Total Reflection-Fourier Transform Infrared (ATR-FTIR) (Illum and Skaugrud, 1996; Dreher et al., 1997), Differential Scanning Calorimetry (DSC) (Monti et al., 2002; Vaddi et al., 2002), Ramon Spectroscopy (ANC, 1995), etc. Through the above methods, the changes of skin structure, lipid composition and the water content in SC and drug diffusion rate can be observed *ex vivo* and *in vivo* before and after treatment with enhancers. Among these methods, ATR-FTIR has its advantage on elucidating the secondary structure changes of proteins. Therefore, ATR-FTIR has been employed to obtain information about the keratin conformation in SC. After scanned by ATR-FTIR, keratin shows two strong amide absorption peaks in the range of 1700–1500 cm^{-1}, i.e., the amide I absorp-

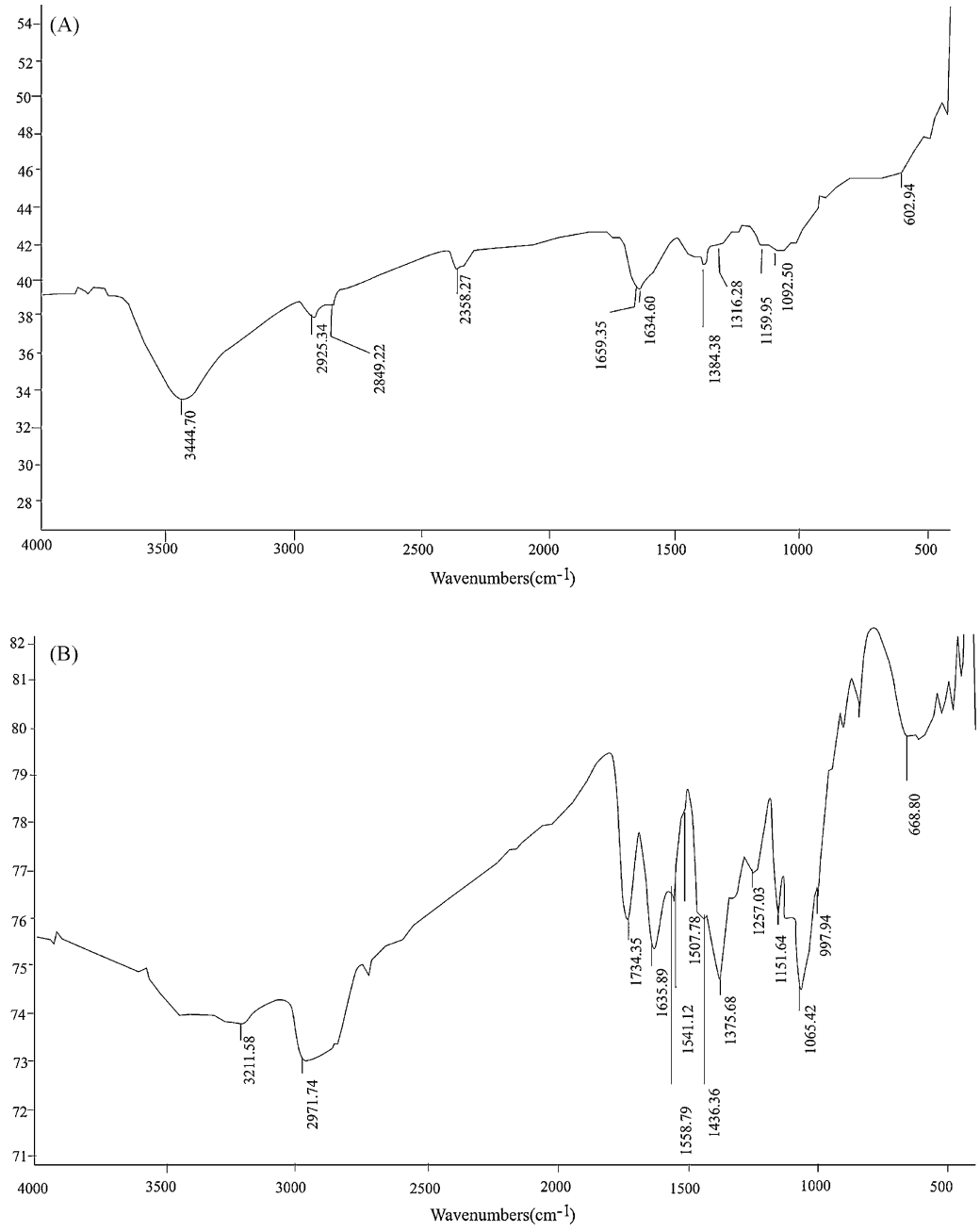

Fig. 2. IR spectra of CS and MCC (A: CS and B: MCC).

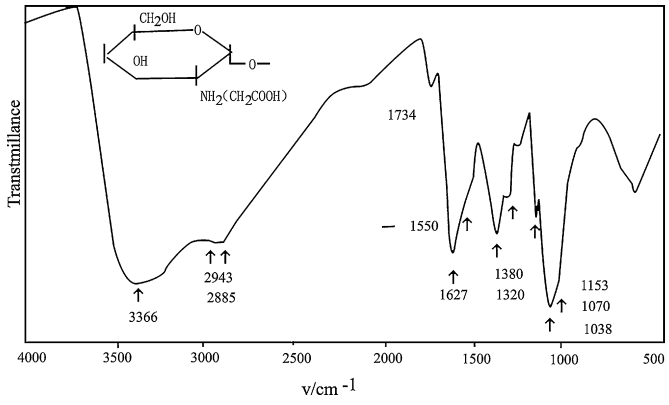

Fig. 3. Standard IR spectrum of MCC.

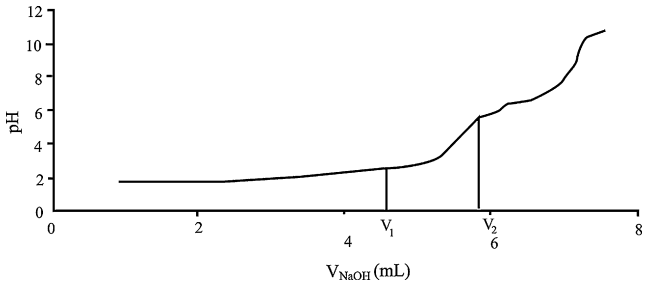

Fig. 4. Titration curve for MCC at 25 °C.

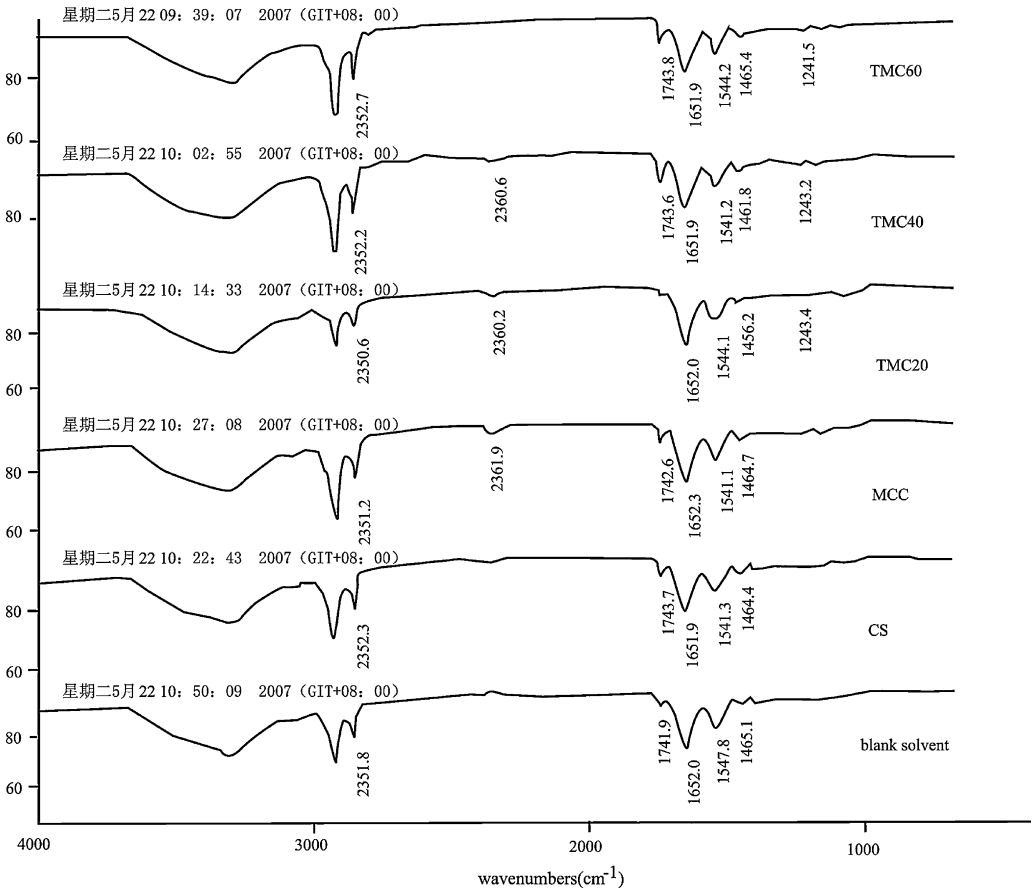

Fig. 5. ATR-FTIR spectra of SC after treated by different agents.

tion peak of 1700–1600 cm^{-1} and the amide II absorption peak of 1600–1500 cm^{-1}. The amide I and amide II absorption peaks are the main indices to evaluate the secondary structure of keratin in SC. Using the amide I absorption peak as a benchmark, the displacement of the amide II absorption peak to lower wavelength was examined to suggest the changes of keratin structure under the effect of enhancers (Dreher et al., 1997; Vitoria et al., 1997; Zbytovska et al., 2004).

Advanced ATR Correction was carried out using OMNIC7.1 program attached by the IR instrument itself and the second-order derivative spectra were obtained using optimal parameters to detect as many component bands as possible (Fig. 5). Two sharp bands at around 1650 and 1540 cm^{-1} corresponded to the absorption of the amide I and amide II, respectively; the peak positions are listed in Table 1. Compared with that of the blank solvent group, the amide II absorption peak of keratin in SC moved to a lower wavelength after treatment with CS, TMCs and MCC.

Table 1
Peak positions of the amide I and amide II of keratin in SC after treatment with various agents.

Samples	Peak position of amide (cm^{-1})	
	I	II
2.5% TMC60	1651.9	1544.2
2.5% TMC40	1651.9	1541.2
2.5% TMC20	1652.0	1544.1
2.5% MCC	1652.3	1541.1
2.5% CS	1651.9	1541.3
Blank solvent	1652.0	1547.8

In the above study, however, the wavelength movement of the amide II absorption peak was so narrow that it was very difficult to define whether the changes arose by CS and its derivatives or just by the error of operation and instrument. Calculated by the second-order derivative, the little shoulder peaks including the strong absorption peaks of the amide I and amide II can be separated to show the tiny changes of the secondary structure of keratin in SC. At the same time, deconvolution combined with curve-fitting technology can increase the surface resolution of spectra and resolve the broad absorption peaks into a group of single peaks. Through fitting, the number, position and area of the single peaks can be obtained (Jiang et al., 1996). However, up till now, there is no standard spectrum of the amide II band to study the frame conformation of polypeptide. In this study, based on the standard spectra of the amide I (Byler and Susi, 1986), the amide I absorption peak was analyzed to elucidate the changes of secondary structure of keratin in SC under the effects of CS, TMCs and MCC. The ranges are: β-sheeting of 1615–1638 cm^{-1}, random coiling of 1638–1645 cm^{-1}, α-helix of 1645–1662 cm^{-1}, and β-turning of 1662–1695 cm^{-1}.

Fourier self-deconvolution and curve-fitting were carried out using Peakfit v4.12 software under the following conditions: Tol% of 9%, deconvolution width of 3.00, filter of 55.0, peak type of spectroscopy and Gauss area and the spectra of SC are shown in Fig. 6. The heights, widths and positions of all bands were optimized successively. The fractional areas of the bands in the amide I region were calculated from the final fitted band areas and the results are shown in Table 2. Under the effect of the blank solvent, the main configuration of amide I was β-turning (49.84%) with β-sheeting (10.04%) and α-helix (3.206%) also present. Upon treatment with CS, TMCs and MCC, the contents of β-sheeting all increased significantly, the contents of β-turning decreased slightly except for

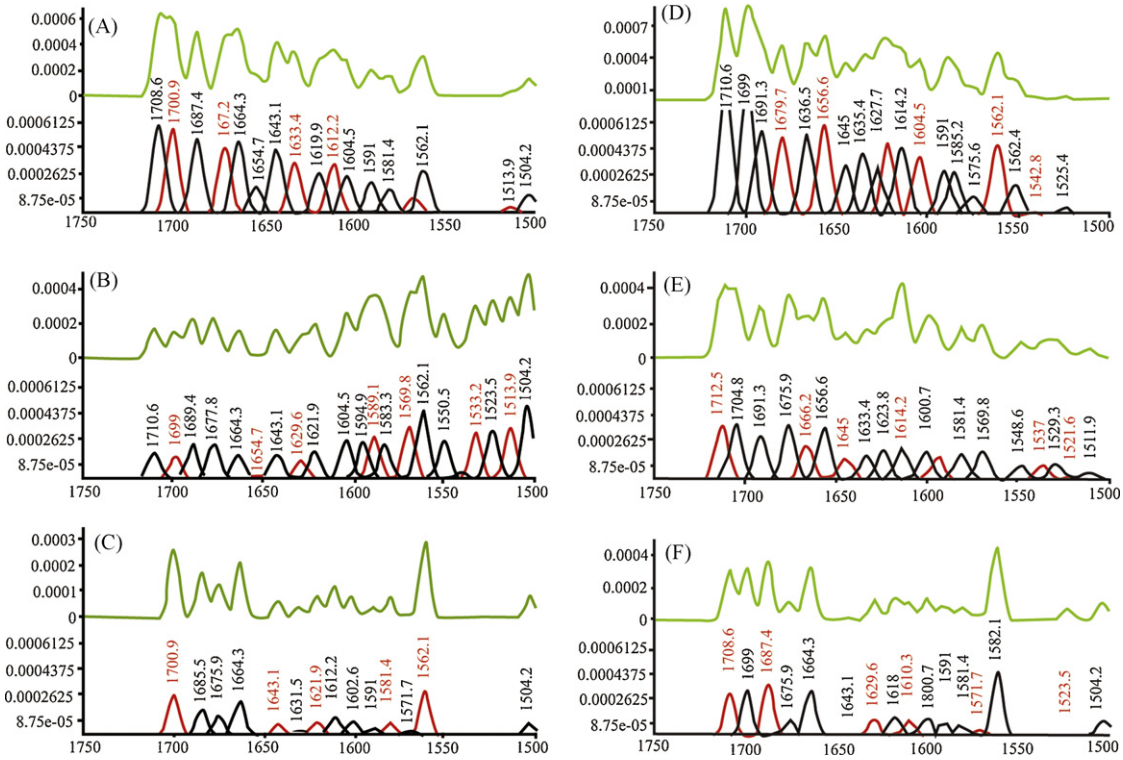

Fig. 6. Deconvolution and curve-fitting spectra of secondary structure of keratin in SC treated by different agents. Upper: deconvolution spectra and under: curve-fitting spectra (A: TMC60; B: TMC40; C: TMC20; D: MCC; E: CS and F: blank solvent).

Table 2
Contents of the secondary structure of keratin in SC after treatment with different agents.

Samples	Content of secondary structure of keratin			
	β-Folding	Random coiling	α-Helix	β-Turning
TMC60	15.75%	6.281%	0	52.34%
TMC40	20.30%	8.891%	0	46.76%
TMC20	16.96%	9.007%	0	48.29%
MCC	22.49%	0	18.53%	35.66%
CS	17.24%	0	21.04%	37.79%
Blank solvent	10.04%	0	3.206%	49.84%

TMC60, and the contents of α-helix vanished completely. Random coiling was observed after the action of TMCs, while the contents of α-helix increased and no random coiling was observed in CS and MCC group.

It suggested that CS and its derivatives could change the secondary structure of keratin in SC leading to more loose accumulative structure of keratin and a larger degree of freedom for carbon movement, which could enhance the transdermal permeation of drugs. The different modes of action of CS, TMCs and MCC on the secondary structure of keratin in SC might be one of the reasons leading to their various enhancing abilities.

3.4. Effects of CS, TMCs and MCC on water content in SC

Besides used in the definition of the secondary structure of proteins, ATR-FTIR was also applied for the water content determination in skin (Gloor et al., 1981). The peak of the amide I shows the absorbance of water and proteins in skin and the amide II only shows the absorbance of proteins in skin. Therefore, the amide I will be strengthened under the effect of water while the amide II will be unchanged. The ratio of the amide I and amide II can be used to show the change of the water content in skin.

The water content in SC was represented by the ratio of amide I absorbance (A_1) and amide II absorbance (A_2) and the results are shown in Fig. 7. Compared with the blank solvent, CS, TMCs

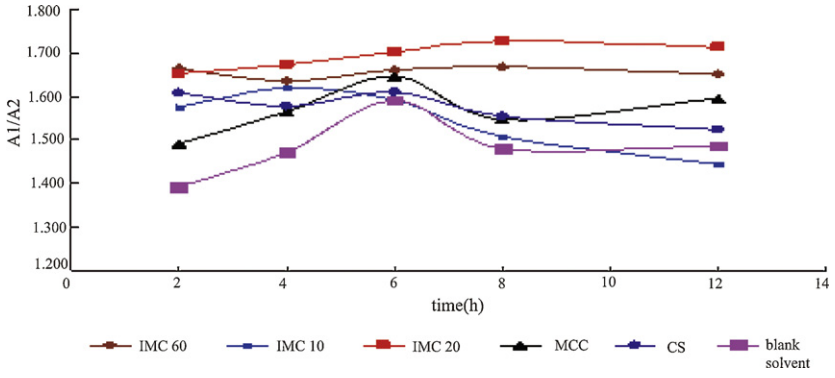

Fig. 7. Effect of CS and its derivatives on the water content in SC.

and MCC all increased the water content significantly in 8 h and decreased it gradually afterwards to exhibit milder changes in the water content of SC during the testing time. TMC40 had the quickest effect for which maximum ratio of A_1/A_2 (1.619) was attained in 4 h, while for that of the other agents, the maximum ratio of A_1/A_2 was obtained in 6 h (CS of 1.610 and MCC of 1.646) or 8 h (TMC20 of 1.728 and TMC60 of 1.669). Among the agents, TMC20 showed the best effect on the increase of the water content of SC with TMC60 showing the next best effect.

During the test, when SC was soaked in the solution of CS and its derivatives, the water could enter the SC to increase the water content in a short time. Combined with their properties of hydroscopicity and 3D network structure, the polysaccharides acted as a storage room for water leading to the increase of the water content in SC and the ability of keeping the water in SC for a longer time.

ATR-FTIR technology is better than the common weighing method used in determining the water content in SC because it can avoid the error of the analytic balance and the sample amount needed is less. However, there is no established linear relationship between A_1/A_2 and the water content up till now. Therefore, through ATR-FTIR method, the actual water amount in SC cannot be determined yet but would be valuable to be studied further in this area.

3.5. Effects of CS, TMCs and MCC on membrane potentials of HaCaT cells

Although Caco-2 cell lines were extensively used as a cell model in the research of mucous membrane absorption, no cell model has been reported to be used in the transdermal penetration. HaCaT cell lines are transformants derived from a human's abdominal epidermal. They are important models for the studies on physiopathology of a human's skin and are generally used as surrogate for formative cells of normal epidermal cutin.

Membrane potential is one of the most important biophysical characters of a cell membrane. It is formed due to the presence of all kinds of pumps in cell membrane to keep the ion concentration gradients inside and outside the cells. The change in membrane potential is always accompanied by the alteration of kinetics and structure of membrane lipid, such as membrane glutinousness, ion permeability, membrane thickness and structure of membrane protein (Zbytovska et al., 2004; Thanou et al., 2000a,b). Nowadays, the techniques often used to study membrane potential are microelectrode intracellular aiming, whole cell patch clamp and fluorescent probe labeling. Among them, the technique of fluorescent probe labeling combined with the detection of flow cytometer attracts much attention due to less cell damage, accurate quantitation and simple operation.

HaCaT cells were fusiformed under a microscope (Fig. 8). A classical spectrum by flow cytometer (TMC20 group) is shown in Fig. 9. The fluorescence intensity of HaCaT cells under the effect of different agents is listed in Table 3. It could be found that after incubation with CS, TMCs and MCC for 30 min, the fluorescence intensity of all

Table 3
Fluorescence intensity of HaCaT cell membrane under the effect of various agents ($n = 5$).

Group	Fluorescence intensity
TMC60	11.95 ± 2.67[#]
TMC40	10.92 + 1.95[#]
TMC20	15.24 ± 2.75[#,*]
MCC	13.10 + 1.20[#]
CS	13.16 + 1.91[#]
Blank D-Hanks solution	8.69 ± 0.68

[#] Compared with blank D-Hanks solution group, $P < 0.05$.
[*] Compared with TMC40 and TMC60 groups, $P < 0.05$.

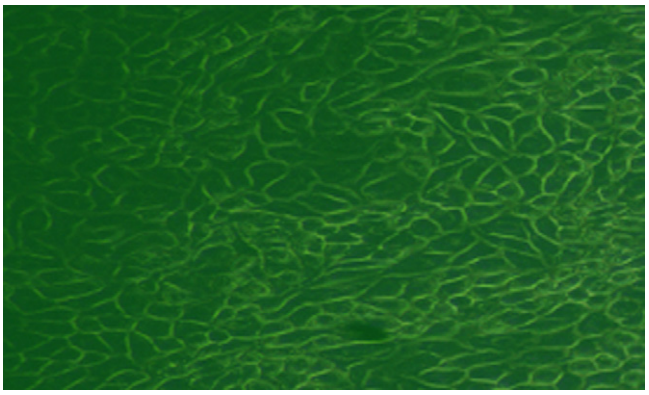

Fig. 8. Photo of HaCaT cells under a microscope(20×).

enhanced significantly indicating the decrease in membrane potential of HaCaT cells as compared to the effect of the blank solvent.

Furthermore, it was found that the effect of TMCs on membrane potential was not DQ-dependent which disagreed with the action mode of their absorption enhancement on epithelial cells. Here, TMC20 appeared to decrease membrane potentials in a more pronounced way than TMC60 and TMC40, and the effect of TMC40 was the weakest. The same pattern was also observed in their enhancing effect on the water content in SC. A presumptive action mode of TMCs on membrane potential is shown in Fig. 10. In resting state, the inside of cell membrane was negatively charged and the outside was positively charged. When TMCs acted on cell membrane, they could cause a depolarization of membrane and form an electric field. As the fluorescent probe was negatively charged, it could be transported across the membrane under the driving force of the electric field. The action intensity of TMCs on cell membrane was DQ-dependent. The order of charge density of TMCs is TMC60 > TMC40 > TMC20, so the intensity order of depolarization was the same. On the other hand, as TMCs are positively charged, they would weaken the "intensity of the electric field" leading to the decrease of the fluorescent probe transportation, which could be called "negative compensation". The order of the intensity of negative compensation is the same as above, so the negative compensation of TMC20 was the least. The eventual effect of TMCs on the cell membrane potential might be the result of the combination of depolarization and negative compensation leading to the order of TMC20 > TMC60 > TMC40 for their effect on cell membrane potential.

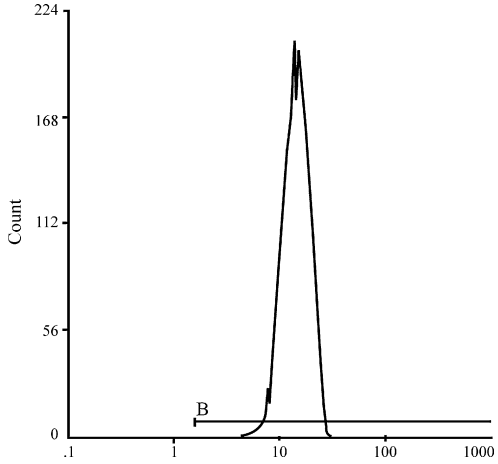

Fig. 9. Classic spectrum of the result by the flow cytometer (TMC20 group).

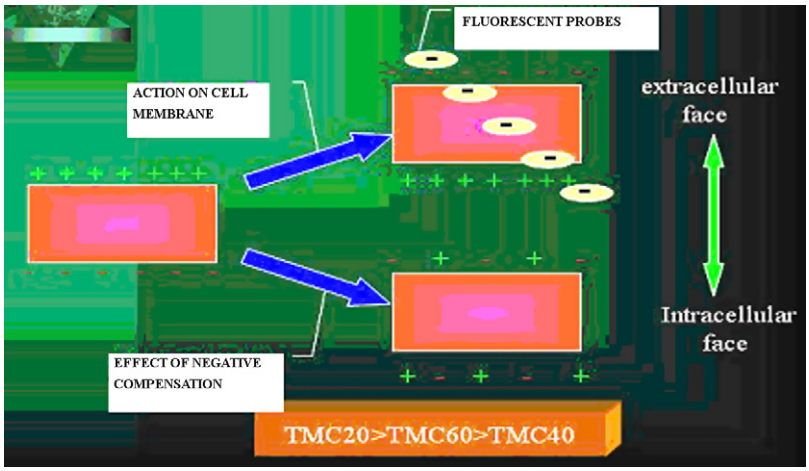

Fig. 10. Presumptive action pattern of TMCs on membrane potentials of HaCaT cells.

3.6. Changes in membrane fluidity of HaCaT cells under the effect of CS, TMCs and MCC

The lipids and proteins in the cell membrane possess certain fluidity. The changes in the cell membrane fluidity could cause many functional alterations of the cells, such as transmembrane transportation, membrane-bound enzyme activity, binding of ligand and membrane receptor, cell differentiation and cell recognization (Shiniztky, 1984). The technique of FRAP has been used to study the lateral mobility of membrane lipids and proteins in a variety of cells and tissues (Juan et al., 1982). Combined with a laser scanning confocal microscope, FRAP can analyze membrane composition of living cells and developing changes in cytoplasmic structure without damaging the cells. The operation process is also simple. First, membrane phospholipids are labeled by a fluorescent probe NBD-C6-HPC. Next a certain area on the surface of the living cell is radiated by high-intensity laser beams in order to bleach the fluorescence. After that, due to membrane fluidity, the fluorescence probe from the other area can move to the photobleaching position leading to the recovery of fluorescence, and the recovery degree can be detected by the radiation of weaker laser beams which suggests the membrane fluidity (Bloch, 1986; Schindler and Jiang, 1987; Van Iwaarden and Van Strijp, 1991).

Fig. 11A shows that the fluorescence on membrane phospholipids of HaCaT cell was green and well-distributed. The chosen area was signed with a circle (R011). After photobleaching, the fluorescence disappeared (Fig. 11B) and the fluorescence recovery happened afterwards at the position of R011 (Fig. 11C). The fluorescence recovery curves under the effect of different agents are shown in Fig. 12 and the recovery rate (*R*%) of each group is listed in Table 4. Compared with that of blank D-Hanks solution, *R*% of CS and its derivatives groups had been increased at different extent suggesting their significant enhancement on cell membrane fluidity. Among them, the effect of CS was the weakest while that of TMC20 was the most significant. The order of *R*% in different groups was TMC20 > TMC60 > TMC40 > MCC > CS. Thus, the structure reforming at 2-N position in CS seems to not only improve the solubility of CS, but also increase the enhancement on cell membrane mobility. Interestingly, the *R*% order of TMCs was the same as that of their effect on cell membrane potential. The combination effect of depolarization and negative compensation might also be suitable to explain the result here.

Table 4
Fluorescence recovery rate (*R*%) after treatment with various agents.

Group	*R* (%)
Blank D-Hanks solution	25.8%
CS	41.3%*
MCC	51.7%*
TMC20	78.3%*
TMC40	57.4%*
TMC60	61.5%*

* Compared with blank D-Hanks solution group, $P < 0.05$.

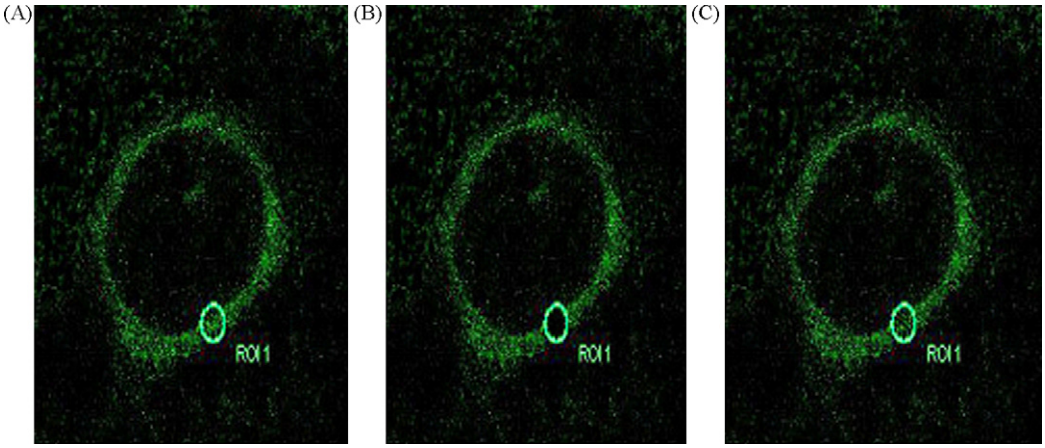

Fig. 11. Fluorescence images of membrane phospholipids of HaCaT cell by tomoscan (A: before photobleaching; B: after photobleaching and C: fluorescence recovery after photobleaching).

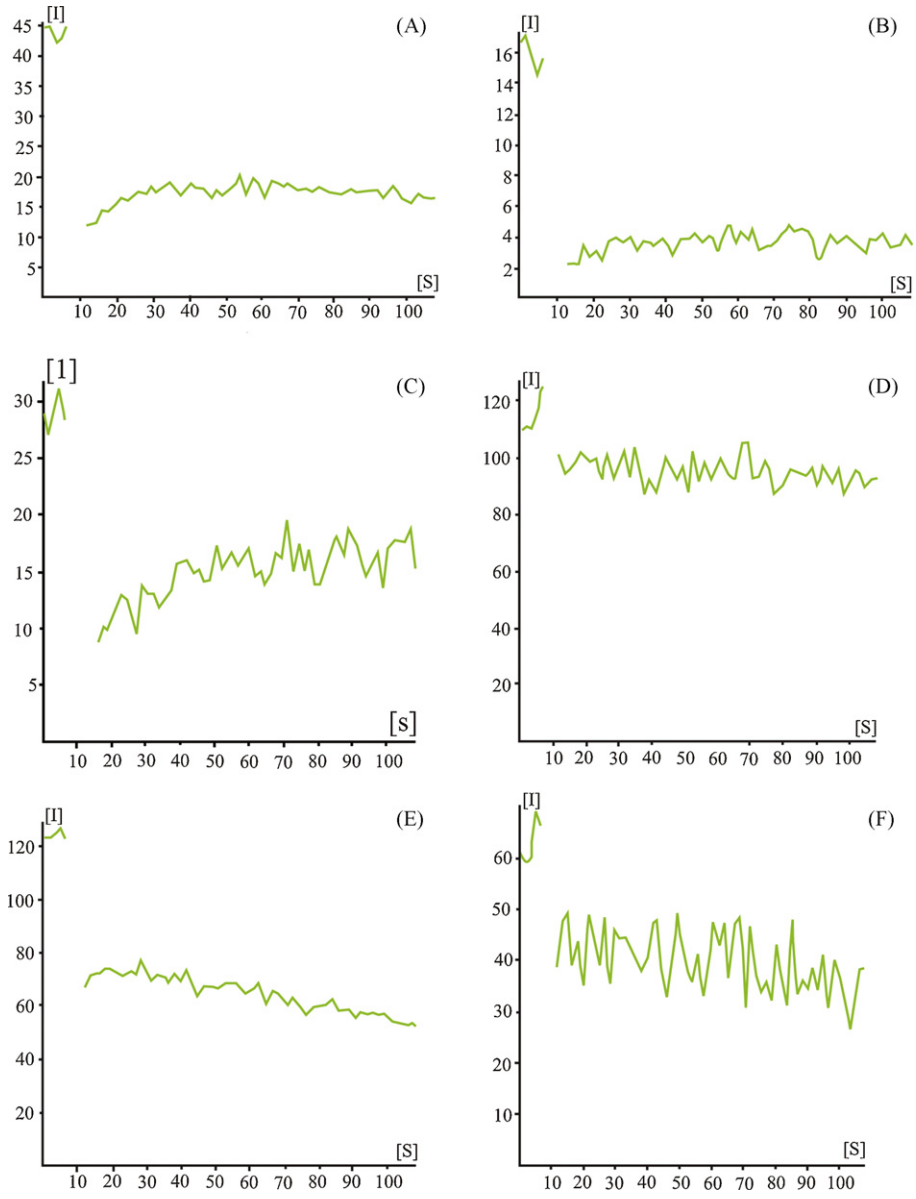

Fig. 12. Fluorescence recovery curves under the effect of different agents (A: blank D-Hanks solution; B: CS; C: MCC; D: TMC20; E: TMC40 and F: TMC60).

4. Conclusions

Our previous studies have shown that TMCs could prominently increase the drug transdermal penetration *in vitro* and *in vivo*. In this study, the mechanisms of transdermal enhancement of CS, TMCs and MCC were investigated by various techniques. It was found that CS and its derivatives could significantly change the secondary structure of keratin in SC, increase the water content in SC, decrease HaCaT cell membrane potential and enhance cell membrane fluidity to various degrees. We believe that this study is the first to demonstrate the mechanisms of transdermal enhancement of CS, TMCs and MCC. This may be a foundation for a further study of the transdermal enhancement of CS and its derivatives.

References

ANC, A., 1995. Fourier transforms Raman spectroscopy of interactions between the penetration enhancer dimethyl sulfoxide and human stratum coreum. Int. J. Pharm. 265, 228–243.

Bloch, E.R., 1986. Fluidity in microbody membrane. J. Appl. Physiol. 60, 826–835.

Byler, D.M., Susi, H., 1986. Examination of the secondary structure of proteins by deconvolved FTIR spectra. Biopolymers 25, 469–487.

Daughety, A.L., Mrsny, R.L., 1999. Regulation of the intestinal epithelial paracelluar barrier. Pharm. Sci. Technol. Today 2, 281–287.

De Graaff, A.M., Li, G.L., Van Aelst, A.C., Bouwstraa, J.A., 2003. Combined chemical and electrical enhancement modulates stratum corneum structure. J. Control. Release 90, 49–58.

Di Colo, G., Burgalassi, S., Zambito, Y., Nardini, I., Saettone, M.F., 2004. Effect of chitosan and of N-carboxymethylchitosan on intraocular penetration of topically applied ofloxacin. Int. J. Pharm. 273, 37–44.

Dreher, F., Walde, R., Walther, R., Wehrli, E., 1997. Interaction of a lecithin microemulsion gel with human stratum corneum and its effect on transdermal transport. J. Control. Release 45, 131–140.

Giuseppina, S., Silvia, R., Maria, C.B., Franca, F., Ylenia, Z., Giacomo, D.C., Carla, C., 2005. Buccal penetration enhancement properties of N-trimethyl chitosan: influence of quaternization degree on absorption of a high molecular weight molecule. Int. J. Pharm. 297, 146–155.

Gloor, M., Hirsch, G., Willebrandt, U., 1981. On the use of infrared spectroscopy for the in vivo measurement of the water content of the horny layer after application of dermatologic ointments. Arch. Dermatol. Res. 271, 305–313.

Hamman, J.H., Kotze, A.F., 2001. Effect of the type of base and number of reaction steps on the degree of quaternization and molecular weight of *N*-trimethyl chitosan chloride. Drug Dev. Ind. Pharm. 27, 373–380.

Hamman, J.H., Stander, M., Kotze, A.F., Monti, D., Chetoni, P.J., 2002. Effect of degree of quaternization of *N*-trimethyl chitosan chloride on absorption enhancement: in vivo evaluation in rat nasal epithelia. Int. J. Pharm. 232, 235–242.

Illum, L., Skaugrud, T.J.A., 1996. Chitosan as a nasal delivery system: evaluation of insulin absorption enhancement and effect on nasal membrane integrity using rat models. Eur. J. Pharm. Sci. 4, 23–31.
Jiang, H.l., Song, Z.J., Ling, M.S., Zhang, D., 1996. FTIR studies of recombinant human granulocyte-macrophrage colony-stimulating factor in aqueous solutions: secondary structure, disulfide reduction and thermal behavior. Biochem. Biophys. Acta 1294, 121–128.
Jonker, C., Hamman, J.H., Kotze, A.F., 2002. Intestinal paracellular permeation enhancement with quaternized chitosan: in situ and in vitro evaluation. Int. J. Pharm. 238, 205–213.
Juan, Y., Jeffrey, A.S., Evangelina, E.Y., 1982. Lateral mobility in membranes as detected by fluorescence recovery after photobleaching. Biophys. J. Biophys. Soc. 39, 69–75.
Junginger, H.E., Verhoef, J.C., 1998. Macromolecules as safe penetration enhancers for hydrophilic drugs—a fiction? PSTT 1, 370–376.
Kotze, A.F., Thanou, M.M., Luesen, H.L., Boer, A.G.de., Verhoef, J.C., Junginger, H.E., 1999. Enhancement of paracellular drug transport with highly quaternized N-trimethyl chitosan chloride in neutral environments: in vitro evaluation in intestinal epithelial cells (Caco-2). J. Pharm. Sci. 88, 253–257.
Kuljit, S., Bhatia, J.S., 1999. Effect of linolenic acid:ethanol or limonene:ethanol and iontophoresis on the in vitro percutaneous absorption of LHRH and ultrastructure of human epidermis. Int. J. Pharm. 180, 235–250.
Liu, C.X., Chen, G.H., Jin, Z.T., 2004. Modification of the formula for calculation of substitution degree of N,O-carboxymethyl chitosan. J. Beijing Univ. Chem. Technol. 31, 14–17.
Monti, D.S., Burgalassi, P.C., Najarro, M., Saettone, M.F., 2002. Increased corneal hydration induced by potential ocular penetration enhancers: assessment by differential scanning calorimetry (DSC) and by desiccation. Int. J. Pharm. 232, 139–147.
Riccardo, A.A., Muzzarelli, Tanfani, F., Emanuelli, M., Mariotti, S., 1982. N-(carboxymethylidene) chitosans and N-(carboxymethyl)-chitosans: novel chelating polyampholytes obtained from chitosan glyoxylate. Carbohydr. Res. 107, 199–214.
Schindler, M., Jiang, L.W., 1987. Fluorescence redistribution after photobleaching as a tool for dissecting the control elements of nucleocytoplasmic transport. Methods Enzymol. 141, 447–459.
Shiniztky, M., 1984. Membrane fluidity and cellular functions. In: Shinitzky, M. (Ed.), Physiology of Membrane Fluidity. CRC, Boca Raton, FL, pp. 1–51.
Sinswat, P., Tengamnuay, P., 2003. Enhancing effect of chitosan on nasal absorption of salmon calcitonin in rats: comparison with hydroxypropyl- and dimethyl-β-cyclodextrins. Int. J. Pharm. 257, 15–22.
Snyman, D., Hamman, J.H., Kotze, J.S., Rollings, J.E., Kotze, A.F., 2001. The relationship between absolute molecular weight and the degree of quaternization of N-trimethyl chitosan chloride. Carbohydr. Res. 50, 145–150.
Taveira, S.F., Nomizo, A., Lopez, R.F.V., 2009. Effect of the iontophoresis of a chitosan gel on doxorubicin skin penetration and cytotoxicity. J Control. Release 134, 35–40.
Thanou, M.M., Florea, B.I., Langemeyer, M.W.E., Verhoef, J.C., Junginger, H.E., 2000a. N-trimethylated chitosan chloride (TMC) improves the intestinal permeation of the peptide drug buserelin in vitro (Caco-2) and in vivo (rats). Pharm. Res. 17, 27–31.
Thanou, M.M., Verhoef, J.C., Junginger, H.E., 2001. Oral drug absorption enhancement by chitosan and its derivatives. Adv. Drug Deliv. Res. 52, 117–126.
Thanou, M.M., Kotze, A.F., Scharringhausen, T., Lueben, H.L., 2000b. Effect of degree of quaternization of N-trimethyl chitosan chloride for enhanced transport of hydrophilic compounds across intestinal Caco-2 cell monolayers. J. Control. Release 64, 15–25.
Vaddi, H.K., Ho, P.C., Chan, Y.W., Chana, S.Y., 2002. Terpenes in ethanol: haloperidol permeation and partition through human skin and stratum corneum changes. J. Control. Release 81, 121–133.
Van Iwaarden, J.F., Van Strijp, J.A.G., 1991. Surfactant protein A is opsonin in phagocytosis of herpes simplex virus type 1 by rat alveolar macrophages. Am. Physiol. Soc., L204–L209.
Vitoria, M., Bentley, L.B., Kedor, E.R.M., Vianna, R.F., Collett, J.H., 1997. The influence of lecithin and urea on the in vitro permeation of hydrocortisone acetate through skin from hairless mouse. Int. J. Pharm. 146, 255–262.
Wen, H., Xianxi, G., Mian, Z., 2008. Transdermal permeation enhancement of N-trimethyl chitosan for testosterone. Int. J. Pharm. 356, 82–87.
Zbytovska, J., Raudenkolb, S., Wartewig, S., 2004. Phase behavior of transkarbam 12. Chem. Phys. Lipids 129, 97–109.